Front. Earth Sci. 2022, 16(2): 465–482
https://doi.org/10.1007/s11707-021-0901-1

RESEARCH ARTICLE

Study of corrosion mechanism of dawsonite led by CO_2 partial pressure

Fulai LI (✉)[1,2], Hao DIAO[1,2], Wenkuan MA[1,2], Maozhen WANG[3]

1 Shandong Provincial Key Laboratory of Deep Oil and Gas, School of Geosciences, China University of Petroleum (East China), Qingdao 266580, China
2 Laboratory for Marine Mineral Resources, Qingdao National Laboratory for Marine Science and Technology, Qingdao 266071, China
3 Bohai Oilfield Research Institute, Tianjin Branch of CNOOC China Limited, Tianjin 300452, China

Abstract The stability of dawsonite is an important factor affecting the feasibility evaluation of CO_2 geological storage. In this paper, a series of experiments on the interaction of CO_2-water-dawsonite-bearing sandstone were carried out under different CO_2 pressures. Considering the dissolution morphology and element composition of dawsonite after the experiment and the fluid evolution in equilibrium with dawsonite, the corrosion mechanism of dawsonite led by CO_2 partial pressure was discussed. The CO_2 fugacity of the vapor phase in the system was calculated using the Peng–Robinson equation of state combined with the van der Waals 1-fluid mixing rule. The experimental results indicated that the thermodynamic stability of dawsonite increased with the increase of CO_2 partial pressure and decreased with the increase of temperature. The temperature at which dawsonite dissolution occurred was higher at higher f_{CO_2}. There were two different ways to reduce dawsonite's stability: the transformation of constituent elements and crystal structure damage. Dawsonite undergoes component element transformation and crystal structure damage under different CO_2 pressures with certain temperature limits. Based on the comparison of the corrosion temperature of dawsonite, three corrosion evolution models of dawsonite under low, medium, and high CO_2 pressures were summarized. Under conditions of medium and low CO_2 pressure, as the temperature continued to increase and exceeded its stability limit, the dawsonite crystal structure was corroded first. Then the constituent elements of dawsonite dissolved, and the transformation of dawsonite to gibbsite began. At high CO_2 pressure, the constituent elements of dawsonite dissolved first with the increase of temperature, forming gibbsite, followed by the corrosion of crystalline structure.

Received June 1, 2020; accepted February 24, 2021

E-mail: liful@upc.edu.cn

Keywords dawsonite stability, CO_2-water-rock interaction, corrosion mechanism, CO_2 geological storage

1 Introduction

Climate warming, glacier melting, level sea rise, and the resulting extinction have been the most discussed topics in recent years (Karl et al., 2009; Dejean et al., 2011; Liu et al., 2012; Melillo, 2014; Gunnemyr, 2019). This series of thought-provoking problems are caused by the continuous increase of atmospheric greenhouse gases, mainly carbon dioxide (CO_2) resulting from human factors (Karl and Trenberth, 2003). The fifth IPCC assessment report (AR5) points out that the changes in human usage of fossil fuels and land usage have caused a significant increase in atmospheric CO_2 concentration (IPCC, 2014). In addition to curbing greenhouse gas emissions, the geological storage of CO_2 is considered an essential approach (Holloway, 2005; Zerai et al., 2006; Benson and Cole, 2008; Oelkers and Cole, 2008; Aminu et al., 2017; Ajayi et al., 2019), and large-scale pilot projects have been carried out in many places (Korbøl and Kaddour, 1995; Holloway, 2005; Kharaka et al., 2006; Shevalier et al., 2009). Geological storage of CO_2 is to inject CO_2 into the underground unrecoverable coal seam, depleted oil and gas reservoir, and deep saline layer (Bachu, 2002; Xu et al., 2004; Jiang et al., 2008; Aminu et al., 2017; Bakhshi et al., 2018; Ajayi et al., 2019) in a supercritical state. This process involves the interaction between CO_2, formation fluid, and rock. CO_2 is sealed in the underground stratum in the form of dissolved capture, structural storage, and mineral capture (Oelkers and Cole, 2008; DePaolo and Cole, 2013; Li et al., 2017; Bakhshi et al., 2018; Yu et al., 2019; Yuan et al., 2019). Mineral capture is considered the main form of CO_2 "permanent" storage, with a time scale of up to 1000 years (Jiang et al., 2008). After CO_2 being

injected into the stratum, carbon fixation minerals such as siderite, magnesite, ankerite, and dawsonite can be generated through the interaction with formation rocks and fluids (Gao et al., 2008; Gysi and Stefánsson, 2008; Lechat et al., 2016; Li et al., 2017; Yang et al., 2018a; Yuan et al., 2019; Raza et al., 2018; Elidemir and Güleç, 2018). Among them, dawsonite is considered a tracer mineral for CO_2 charging, accumulation, or dispersing (Gao and Liu, 2006; Dong et al., 2009; Gao et al., 2009; Yu et al., 2019) and is also a major trap mineral for CO_2 in the stratum (Moore et al., 2005; Worden, 2006; Zhou et al., 2014; Li et al., 2017). Therefore, understanding the mineral's stability is of great significance for the selection of a CO_2 geological storage site and the long-term safety of the project.

Dawsonite was thought to form in high CO_2 partial pressure (e.g., Xu et al., 2003; Zhang et al., 2004; Álvarez-Ayuso and Nugteren, 2005; Okuyama et al., 2011), the temperature between 25°C–100°C (Chesworth, 1971; Baker et al., 1995; Álvarez-Ayuso and Nugteren, 2005; Gao and Liu, 2006; Worden, 2006; Li et al., 2018), in alkaline fluid rich in sodium and aluminum (Johnson et al., 2004; Johnson, 2009; Gaus, 2010; Wang et al., 2016; Li et al., 2017). The production site was mainly associated with CO_2 gas reservoirs or adjacent sandstone formations (Okuyama, 2014; Zhou et al., 2014; Li and Li, 2017). Previous studies on dawsonite-bearing sandstone in Dongying Sag conducted by Li et al. (2018) showed that the maximum temperature that dawsonite in 4.3 MPa CO_2 pressure can maintain its stability was 120°C. But the formation temperature is lower than 80°C, which means that the high CO_2 pressure in the stratum can maintain the stable preservation of dawsonite. However, the CO_2 pressure maintained in the underground stratum is restricted by many factors, such as sealing layer, fault, rock property, and fluid activity. In the process of geological storage, the pressure of CO_2 in the stratum will keep decreasing with time, so there is a problem: what is the state of dawsonite when the pressure of CO_2 is low, or the pressure of CO_2 is zero? On the other hand, CO_2 initially injected into the stratum is in a supercritical state with relatively high pressure. CO_2 under this condition is a gas-liquid mixed-phase and with both gas and liquid properties (Holloway and Savage, 1993). CO_2 in this state has a density close to that of a liquid. It also has a viscosity coefficient and a diffusion coefficient close to that of a gas. CO_2's high fluidity and transmission characteristics under this condition can meet the requirement to store large amounts of CO_2 in geological storage projects. However, the CO_2 in this state is extremely unstable, and its effect on the formed dawsonite is not completely understood. Therefore, the purpose of this research is to 1) study the preservation conditions of dawsonite under low, medium, and high CO_2 pressures, respectively; 2) analyze the corrosion mechanism of dawsonite under different CO_2 pressures and temperature conditions. This study provides a new understanding of dawsonite's stability and a new basis for the feasibility evaluation of the CO_2 geological storage.

2 Materials and methods

2.1 Sample selection

In this study, the Paleogene Shahejie Formation in Binnan area of Dongying Depression was selected as the study object. Optical identification of sandstone samples was performed under OLYMPUS polarizing microscope. The petrological analysis of the clastic mineral composition of natural sandstone samples was carried out by the point count method (Dickinson, 1970). At least 300 points were collected for each thin section. The selected samples are fine sandstone mainly composed of quartz (45.97%), feldspar (20.52%), rock fragment (13.3%), and carbonate cement (13.84%, mainly dawsonite). Before the experiment, the sandstone sample was made into a cylindrical shape with a radius of about 1 cm and a thickness of 2–3 mm. One side was polished, and the other side was marked. The sample was divided into four fan-shaped parts to meet the sample volume requirements of all experiments. The reaction solution used in each group was 350 mL distilled water. The CO_2 gas used in each experiment was high-purity CO_2 with a purity higher than 99.995%.

2.2 Experimental set-up

In this study, laboratory reactor experiments were used to simulate different temperatures and CO_2 partial pressures that natural dawsonite (dawsonite formed after CO_2 injection into the formation) might experience in the formation. In different pressures (by injecting compressed CO_2 gas) and temperatures, eight experiments were conducted under the condition of normal pressure (without CO_2 injected) 80/100°C, 4 MPa 80/100/120°C, and 7.3 MPa 120/140/160°C. In each experiment group, two sandstone samples were placed for SEM, EDS, and XRD, respectively, and they were weighed before and after the experiment. The experimental instruments were mainly composed of a stainless-steel alloy reactor, gas booster system, oil-free air compressor, gas source, and automatic control system (Fig. 1). An experiment of normal pressure had no CO_2 injected, which was conducted with directly raising of the temperature of the reactor to the experimental temperature by an automatic control system (temperature deviation in the ±1°C). The CO_2 used in experiments with pressures of 4 MPa and 7.3 MPa was provided by a gas source. The reactor was then raised to the experimental state by an oil-free air compressor and gas booster system (pressure deviation in the ±0.1 MPa), after which the temperature of the reactor was raised to the experimental temperature by an automatic control system (temperature

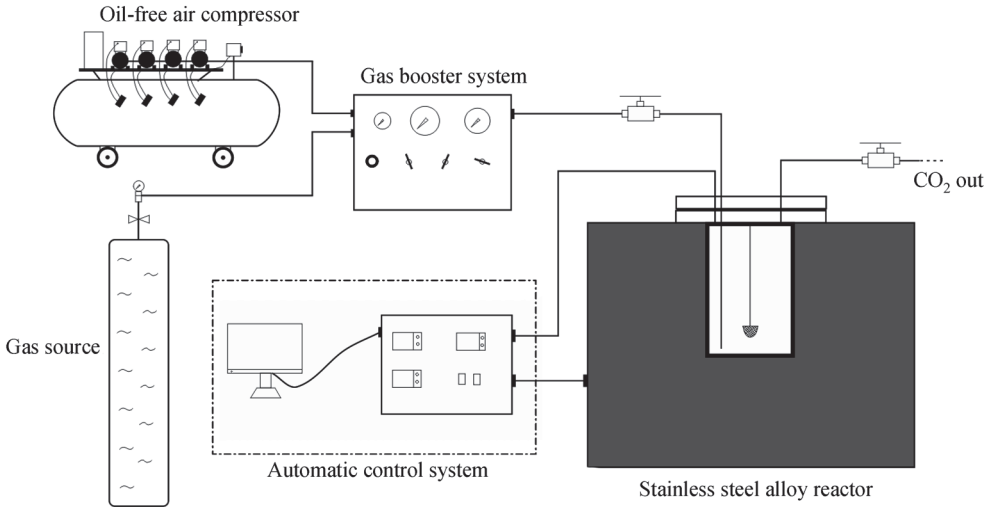

Fig. 1 Laboratory apparatus used for water-rock-CO_2 reactions.

deviation is in ±1°C). Each group of experiments was set to 72 h, during which temperature and pressure in the reactor were monitored through the temperature and pressure sensor component of the automatic control system, and temperature and pressure data on its display screen were recorded every two hours to ensure that the reaction was carried out at a constant temperature and pressure. After the reaction was over, the solution was cooled to room temperature, and the solution was removed with a disposable straw and stored in a non-polluting plastic bottle. Finally, the solid samples were removed, washed, and dried (60°C, 24 h). The weighing of the solid sample was carried out on an electronic balance with an accuracy of 0.001 g.

2.3 Analytical methods

After the experiment, scanning electron microscopy observation and energy spectrum analysis were performed on 9 solid samples, including one original sample and eight experimental samples. Six samples were tested in the Formation and Paleontology Research Center of Jilin University using JMS-6700S field emission electron microscopy and an INCAX- SIGHT spectrometer. The other three samples were tested in the first Marine Research Institute of the State Oceanic Administration using a Quanta 200 scanning electron microscope and EDAX Genesis 2000 spectrometer. The morphology of each mineral in the sandstone sample was observed under the scanning electron microscope, and the mineral composition was analyzed with the energy spectrum probe. In addition, X-ray diffraction analysis was performed on the remaining nine sandstone samples to determine the content of major minerals in the samples. The test was carried out using a D/max-2500 X-ray diffractometer at the State Key Laboratory of Heavy Oil of the China University of Petroleum (East China). Before the analysis, the sample was initially crushed with a copper bowl, and the sample was further grounded to less than 40 um using an agate cup to fully separate the sandstone sample. The diffractometer used Cu as the radioactive source, and the current and voltage were 40 mA and 40 kV, respectively. Samples were scanned from 5° to 61° in the step length of 0.017°. The hydrochemical analysis of the reaction solution was carried out in the Institute of Geology and Geophysics, Chinese Academy of Sciences. The pH value of the solution after the reaction was determined using an AT-510 automatic titration analyzer; the main ion concentration in the solution was detected by an 883 Basic IC plus ion chromatograph, an AT-510 automatic titration analyzer, and an ICS-1100 ion chromatograph, and the concentration of trace elements in the solution was determined by a NexION300D plasma mass spectrometer and a 5300DV plasma emission spectrometer. The measured temperature was 26°C, and the humidity was 61%.

3 Results

3.1 Dissolution of dawsonite-bearing sandstone

3.1.1 Mass loss of sandstone samples

The interaction of CO_2-water-sandstone can lead to the dissolution of sandstone, resulting in its mass reduction. The experimental pressures and temperatures of the research were normal pressure (without CO_2 injected) 80/100°C, 4 MPa 80/100/120°C, and 7.3 MPa 120/140/160°C, and the reaction solution used was distilled water with a pH value of 7.

First, under different temperature conditions, CO_2

dissolves in water and reacts with water to form carbonic acid in the first step:

$$CO_2(g) \leftrightarrow CO_2(aq), \quad (1)$$

$$CO_2(aq) + H_2O \leftrightarrow H_2CO_3. \quad (2)$$

The carbonic acid formed by the dissolution of CO_2 in water is weak binary acid, and secondary dissociation will occur:

$$H_2CO_3 \leftrightarrow HCO_3^- + H^+, \quad (3)$$

$$HCO_3^- \leftrightarrow CO_3^{2-} + H^+. \quad (4)$$

The increase of H^+ concentration in an aqueous solution leads to the dissolution of each component in the sandstone. Considering the different mass of solid sandstone samples used in each experiment, this may influence the experimental results and analysis. Therefore, in order to eliminate the influence of this factor, this paper defined mass loss ratio R_m:

$$R_m = \frac{\Delta m}{m_0}, \quad (5)$$

where Δm is the difference in mass of sandstone samples before and after the reaction, and m_0 is the initial mass of sandstone samples. The mass loss ratio of sandstone samples under different CO_2 pressure and temperature conditions was given in Table 1. It can be seen from Fig. 2 that the mass loss ratio of the sandstone sample at normal pressure increased with the increase of temperature, indicating that the degree of dissolution of the sandstone also increased with the increase of temperature, although no CO_2 was injected into the system. The mass loss ratio of sandstone under 4 MPa increased with the increase in temperature first. When the temperature reached 100°C, the mass loss ratio showed a decreasing trend, indicating that the corrosion degree of sandstone samples at a higher temperature was lower than that at a lower temperature. The mass loss ratio of sandstone samples at 7.3 MPa also increased with the increase of temperature, indicating an increase in the degree of dissolution of sandstone.

3.1.2 Mineral composition changes in sandstone samples

Based on the XRD diffraction data of the sandstone samples before and after the reaction, the histogram of the mineral composition of the sandstone samples from different experimental groups was plotted (Fig. 3). It can be seen from Fig. 3(a) that the sandstone sample was mainly composed of quartz, potassium feldspar, calcite, ankerite, dawsonite, and clay minerals and contains a small amount of siderite. Under the experiment of normal pressure (Figs. 3(b) and 3(c)), the percentages of three carbonate minerals, namely, calcite, ankerite, and dawsonite, decreased remarkably with the increase of tempera-

Table 1 Initial reaction conditions and weight loss of samples

Exp.#	T /°C	P /MPa	Initial pH	Time /h	System	Initial solution	Mass before /g	Mass after /g	Mass loss Δm/g	Mass loss rate R_m/%
1	80	0	7	72	Closed	350 mL pure water	1.49	1.47	0.02	1.34
2	100	0	7	72	Closed	350 mL pure water	1.43	1.39	0.04	2.8
3	80	4	7	72	Closed	350 mL pure water	0.62	0.566	0.054	8.71
4	100	4	7	72	Closed	350 mL pure water	0.701	0.622	0.079	11.27
5	120	4	7	72	Closed	350 mL pure water	0.814	0.727	0.087	10.69
6	120	7.3	7	72	Closed	350 mL pure water	0.735	0.675	0.06	8.16
7	140	7.3	7	72	Closed	350 mL pure water	0.902	0.816	0.086	9.53
8	160	7.3	7	72	Closed	350 mL pure water	0.772	0.677	0.095	12.31

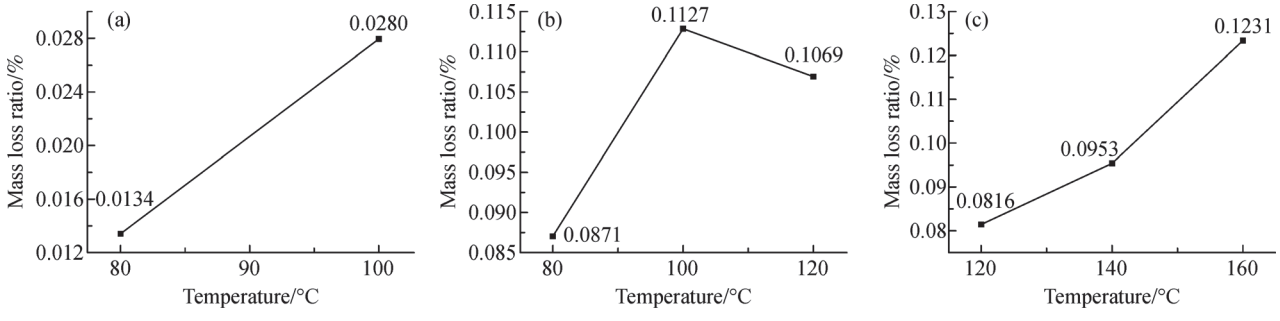

Fig. 2 Mass loss ratio of sandstone samples. (a) Mass loss ratio of sandstone samples at normal pressure; (b) mass loss ratio of sandstone samples at 4 MPa; (c) mass loss ratio of sandstone samples at 7.3 MPa.

ture. The dawsonite content rapidly decreased to zero at the temperature of 80°C. It indicated that while the temperature increased, the content of quartz, K-feldspar, and clay minerals increased, which was not actually due to the regeneration of these minerals in the sandstone. The reason is that quartz, feldspar, and clay minerals in sandstone have higher stability relative to carbonate minerals, and their dissolution rate is relatively slow (Arvidson et al., 2003; Kampman et al., 2009). Under experimental pressure of 4 MPa (Figs. 3(d)–3(f)), the reduction percentage of calcite and ankerite was higher than normal pressure. When the temperature continued to increase from 80°C, the sandstone contained almost no calcite or ankerite. The dawsonite content was relatively lower than normal pressure, but its content gradually decreased to 0 with increasing temperature. Under experimental pressure of 7.3 MPa (Figs. 3(g)–3(i)), the decreasing trend of dawsonite content was slower than that of low pressure, and its content was reduced from 6% at 120°C to 1% at 140°C, and then decreased to 0 at 160°C. The content of calcite, ankerite, and siderite decreased with increasing temperature, and the degree of reduction of siderite was particularly significant. The content of quartz, potassium feldspar, and plagioclase decreased slowly with increasing temperature.

3.2 Hydrochemical characteristics

The CO_2-water-sandstone interactions are visualized as changes in the sandstone's mineral composition (corrosion

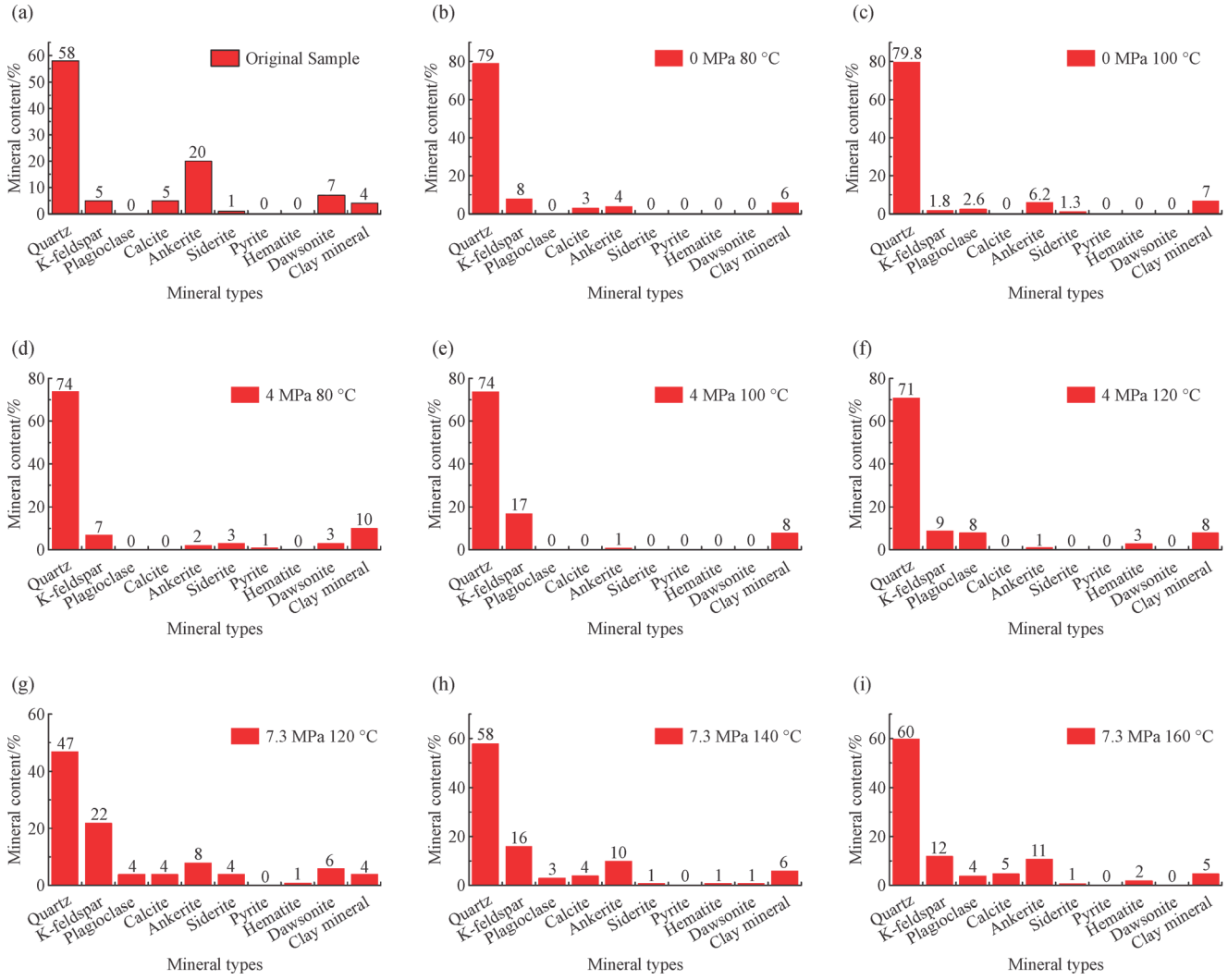

Fig. 3 Mineral composition of sandstone samples. (a) Mineral contents of the original sandstone sample; (b) the content of each mineral in the sandstone sample at normal pressure 80°C; (c) the content of each mineral in the sandstone sample at normal pressure 100°C; (d) the content of each mineral in the sandstone sample at 4 MPa 80°C; (e) the content of each mineral in the sandstone sample at 4 MPa 100°C; (f) the content of each mineral in the sandstone sample at 4 MPa 120°C; (g) the content of each mineral in the sandstone sample at 7.3 MPa 120°C; (h) the content of each mineral in the sandstone sample at 7.3 MPa 140°C; (i) the content of each mineral in the sandstone sample at 7.3 MPa 160°C.

of old minerals and the formation of new minerals) and an increase or decrease in the concentration of anions and cations in the aqueous solution. The change in each ion's concentration in the aqueous solution is caused by released ions when various minerals in the sandstone are dissolved. Therefore, by analyzing the characteristics of each ion concentration's change in the aqueous solution, it is possible to grasp the mineral dissolution information occurring in the sandstone. The concentration of soluble species in solutions after reactions are listed in Table 2.

According to the mineral composition of sandstone, the dissolution reaction of feldspar in the CO_2-water-sandstone reaction is expressed as:

$$KAlSi_3O_{8(K\ feldspar)} + 4H_2O + 4H^+ = K^+ + Al^{3+} + 3H_4SiO_4(aq), \quad (6)$$

$$NaAlSi_3O_{8(albite)} + 4H_2O + 4H^+ = Na^+ + Al^{3+} + 3H_4SiO_4(aq), \quad (7)$$

$$CaAl_2Si_2O_{8(anorthite)} + 8H^+ = Ca^{2+} + 2Al^{3+} + 2H_4SiO_4(aq). \quad (8)$$

The dissolution reaction of calcite, ankerite, and dawsonite is expressed by the following equation:

$$CaCO_{3(calcite)} + H^+ = Ca^{2+} + HCO_3^-, \quad (9)$$

$$Ca(Fe_{0.7}Mg_{0.3})(CO_3)_{2(ankerite)} + 2H^+ = Ca^{2+} + 0.3Mg^{2+} + 0.7Fe^{2+} + 2HCO_3^-, \quad (10)$$

$$NaAlCO_3(OH)_{2(dawsonite)} + 4H^+ = Na^+ + Al^{3+} + CO_2(aq) + 3H_2O. \quad (11)$$

From Eq. (6) to Eq. (11), it is known that K^+ and Na^+ in solution are mainly derived from the dissolution of potassium feldspar and albite. Sources of Ca^{2+} include dissolution from anorthite, calcite, and ankerite. According to XRD data, the content of albite in sandstone is very low, and the content of calcite and ankerite is relatively larger. Therefore, the source of Ca^{2+} is mainly calcite and ankerite. From feldspar dissolution (Eq. (6) to Eq. (8)) and dawsonite dissolution (Eq. (11)), Al^{3+} is the most widely sourced, and the increase in K^+ and Na^+ in solution is certainly less than that of Al^{3+}.

To eliminate the effects of differences in the quality of the starting solid samples for each set of experiments, define the ion dissolution rate u_i:

$$u_i = \frac{C_i \times V}{m_0}, \quad (12)$$

wherein C_i (mg/L) is the ion concentration of the ion i in the solution after the reaction, V (L) is the volume of the reaction solution, and m_0 (mg) is the initial mass of the solid sample. u_i represents the ratio of the mass of the ion i in the solution to the mass of the starting solid sample. It eliminates the influence of the difference in the quality of the starting sample under different experimental conditions. The larger the value, the higher the increase of the ion in the solution after the reaction.

Figure 4 shows changes in the ion dissolution rate of each anion and cation in the solution after the reaction. Among them, to better display the variation characteristics of all ions, the ion dissolution rate with a huge difference in individual values is scaled (multiplied or divided by a multiple of 10), which is more conducive to analyzing the change of ions in the solution. At the experiment of normal pressure, the dissolution rates of Ca^{2+} and Fe^{2+} ions released from the dissolution of calcite and ankerite were significantly increased (Figs. 4(a) and 4(b)). The dissolution rate of K^+ also showed an upward trend, but it was relatively slow. Contrary to the increasing trend of all other cations in the solution, the ion dissolution rate of Al^{3+} tended to decrease, which was contrary to the previous conclusion that the increasing trend of Al^{3+} was more significant than the increasing trend of K^+, Na^+, and Ca^{2+}. It will be explained in detail in Section 4 of this article. At

Table 2 Concentration of soluble species in solutions after reactions

Exp.#	T/°C	Initial pH	P/MPa	Concentration of soluble species/(mg·L^{-1})											
				F	Cl	N	SO	Na	K	Mg	Ca	H.C.	Si	Fe	Al
1	80	7	0	0.08	1.79	0.345	1.42	24.8	0.441	0.608	1.75	73.6	0.175	0.002	0.1
2	100	7	0	0.02	444	0.319	1.02	16.6	0.653	0.662	260	26.5	0.099	0.313	0.018
3	80	7	4	0.12	1.58	1.773	2.07	14.6	0.695	17.4	50.9	263	2.07	0.112	0.02
4	100	7	4	0.08	1.72	0.675	2.14	60.7	1.1	12.4	40.1	328	1.42	0.102	0.017
5	120	7	4	0.08	1.46	0.688	2.61	102	2.64	9.76	47.4	447	5.55	0.112	0.019
6	120	7	7.3	0.462	1.08	0.135	21.8	80.8	1.02	7.76	46.6	351	1.68	0.002	0.006
7	140	7	7.3	0.078	1.99	0.204	20.2	101	2.7	10.9	51.9	443	5.52	0.002	0.018
8	160	7	7.3	0.02	0.706	0.097	20.3	117	3.94	7.59	49.8	465	11.8	0.002	0.029

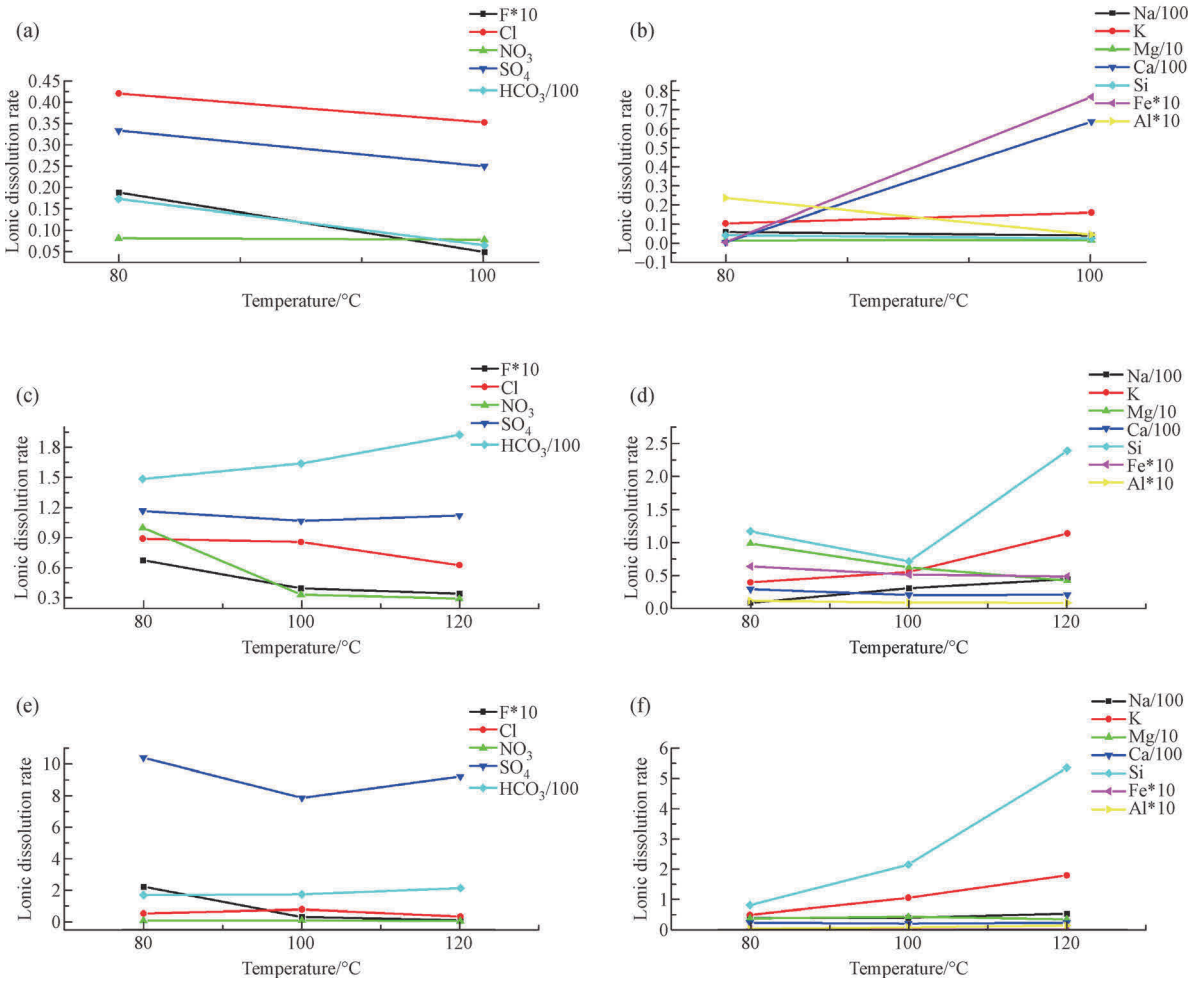

Fig. 4 Ion dissolution rate of each anion and cation in the solution after the reaction. (a) The change of anionic ion dissolution rate with temperature in the reaction solution at normal pressure; (b) the change of cationic ion dissolution rate with temperature in the reaction solution at normal pressure; (c) the change of anionic ion dissolution rate with temperature in the reaction solution at 4 MPa; (d) the change of cationic ion dissolution rate with temperature in the reaction solution at 4 MPa; (e) the change of anionic ion dissolution rate with temperature in the reaction solution at 7.3 MPa; (f) the change of cationic ion dissolution rate with temperature in the reaction solution at 7.3 MPa.

the experimental pressure of 4 MPa, HCO^{3-} showed an increasing trend (Fig. 4(c)). Unlike the case in which the experimental pressure was normal pressure, the HCO^{3-} in the solution at 4 MPa was mainly derived from the dissociation of carbonic acid produced by the dissolution of CO_2 in water. Moreover, as the mineral dissolution reaction continued to consume H^+, the dissociation reaction (Eq. (3)) will promote the increase of HCO^{3-} in the solution in a positive direction. In Fig. 4(d), the ion dissolution rate of K^+, Na^+, and Si-containing ions was significantly increased, while the ion dissolution rate of Al^{3+} was almost zero. A similar result was obtained under the experimental pressure of 7.3 MPa. The ion dissolution rate of K^+ and Si-containing ions showed a significant upward trend in Fig. 4(f). The ion dissolution rate of Al^{3+} was almost always zero, obviously contrary to the previous understanding.

3.3 Corrosion of frame detrital grains

Scanning electron microscopy can be used to visually observe the morphology of each component in sandstone samples under different conditions. At normal pressure 80°C, calcite (Fig. 5(a)) corroded along the cleavage surface to form many dissolved pores and channels, and the dissolution of kaolinite (Fig. 5(b)) was not significant. Potassium feldspar was slightly corroded at normal pressure 100°C (Fig. 5(c)), and the mineral surface only formed a small number of channels along the cleavage; potassium feldspar was further corroded at 4 MPa 80°C (Fig. 5(d)), forming a larger dissolution channel. Albite was significantly corroded at 4 MPa 100°C (Fig. 5(e)). It was strongly corroded along cleavages and formed many channels. Quartz (Fig. 5(f)) did not show significant corrosion at a temperature of 120°C under the experi-

mental pressure of 4 MPa, and the mineral surface was still relatively flat. At 7.3 MPa 120°C, the illite was reticular and only slightly corroded (Fig. 5(g)). At 7.3 MPa 140°C (Fig. 5(h)), the dissolution was more severe, and part of the albite completely dissolved, only part of the residue was retained along the cleavage. At 7.3 MPa 160°C, potassium feldspar (Fig. 5(i)) was violently corroded, and many staggered pores were formed on the mineral surface.

3.4 Dawsonite dissolution

The dawsonite in the original sandstone sample was well preserved, with smooth crystal surfaces and sharp edges (Fig. 6(a)). At normal pressure, when the temperature was 80°C, dawsonite showed that many craters were formed by dissolution, and the surface of the crystal became extremely rough (Fig. 6(b)). When the temperature increased to 100°C, dawsonite was further corroded into a thorn shape, and the degree of dissolution was enhanced. From the root to the outer edge, corrosion was enhanced, and the crystal was severely damaged (Fig. 6(c)). At 4 MPa, when the temperature was 80°C, dawsonite was preserved intact, and no dissolution occurred (Fig. 6(d)). At 100°C, dawsonite still did not undergo significant

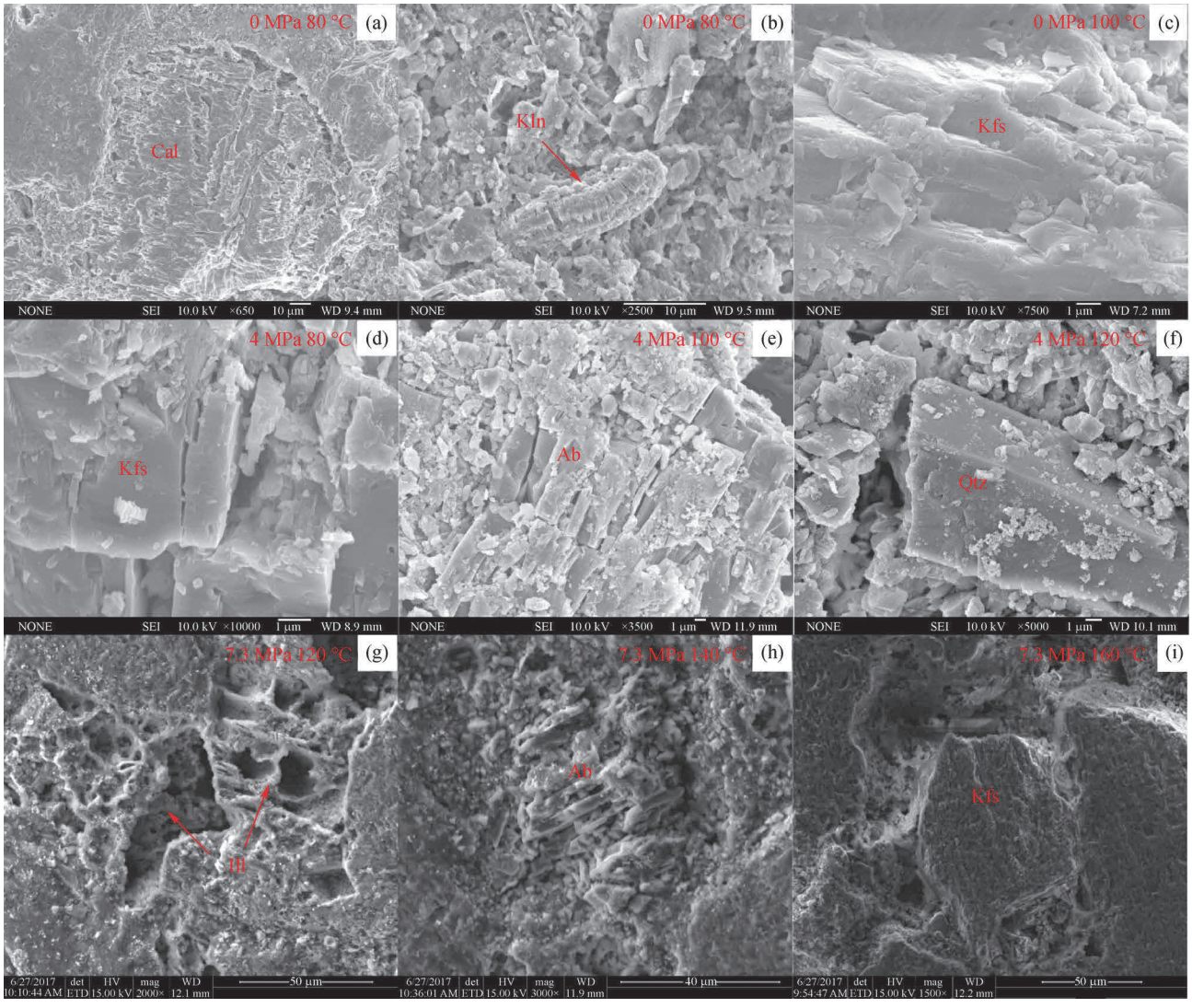

Fig. 5 SEM photos of erosion and dissolution of major minerals in sandstone. (a) Calcite eroded along cleavages, and the surface was eroded to form a large number of pits and channels (normal pressure, T = 80°C); (b) kaolinite is vermiform and only slightly eroded (normal pressure, T = 80°C); (c) slight dissolution of potassium feldspar resulted in tiny pores on the mineral surface and tiny channels along cleavages (normal pressure, T = 100°C); (d) the further dissolution of potassium feldspar, corrosion pits increased, the hole deepened (P = 4 MPa, T = 80°C); (e) albite is obviously eroded, with wide and long channels and large holes on the surface (P = 4 MPa, T = 100°C); (f) the surface of quartz grains is smooth (P = 4 MPa, T = 120°C); (g) illite is reticular and slightly corroded (P = 7.3 MPa, T = 120°C); (h) albite is severely eroded, and the mineral has completely dissolved locally, leaving only some of the residue along the cleavage (P = 7.3 MPa, T = 140°C); (i) dissolution of potassium feldspar, the mineral surface was dissolved along the cleavages and formed a staggered channel (P = 7.3 MPa, T = 160°C). Cal-calcite, kln-kaolinite, kfs-potassium feldspar, Ab-albite, Qtz-quartz, Ill-illite.

dissolution (Fig. 6(e)). At 120°C, dawsonite was corroded, and its individual crystal edges were no longer clear, fine newly precipitated minerals covered the surface, and larger precipitated minerals were formed locally (Fig. 6(f)). The shape of dawsonite aggregation at 7.3 MPa 120°C was still relatively well preserved, but the crystal edges were no longer distinct, and the surface had fine new minerals attached. The outer edge and surface of the crystal began to transform into new minerals. There was good discrimination between the dawsonite crystal (gray-white) and the unconverted dawsonite crystal (gray-black) (Fig. 6(g)). At 7.3 MPa 140°C, the edges of the single crystal in the dawsonite aggregate were more blurred, and the distinction between crystals and the original dawsonite was higher (Fig. 6(h)). At 7.3 MPa 160°C, the dawsonite crystals were almost entirely grayish-white, and the aggregates dissolved from the outer edge of the columnar crystal to the root, resulting in shorter single-crystal lengths (Fig. 6(i)).

The original dawsonite (Fig. 7(a)) without dissolution is composed of C, O, Na, and Al, in which the energy spectrum peaks of O and Al elements are strong, and the energy spectrum peaks of C and Na elements are relatively

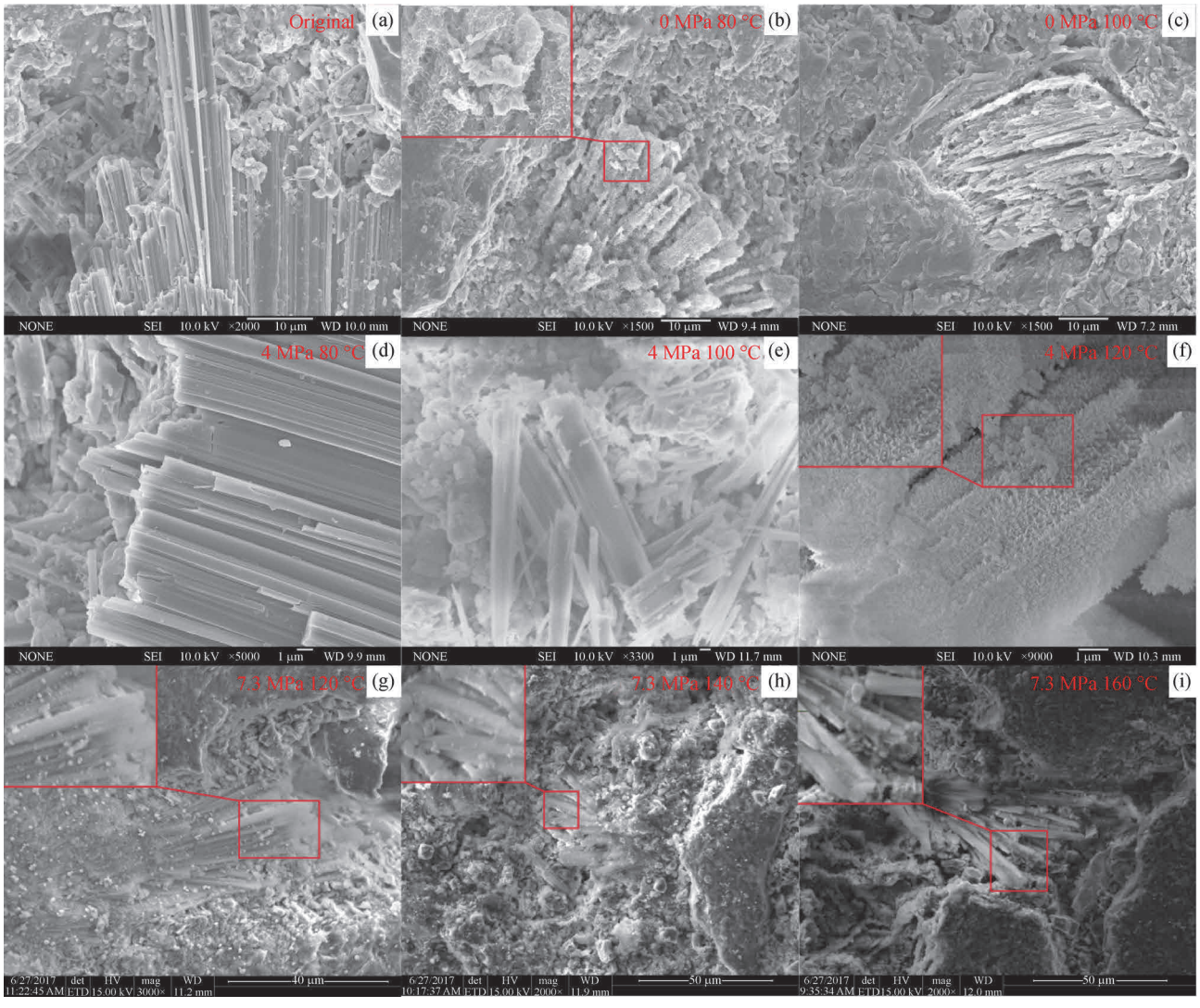

Fig. 6 SEM photos of dawsonite under different experimental conditions. (a) SEM photo of dawsonite in original sandstone; (b) dawsonite eroded significantly, and the surface of the columnar crystal became extremely rough, forming a large number of craters (normal pressure, T = 80°C); (c) dawsonite was further corroded into a thorn shape and the degree of dissolution of dawsonite aggregate was enhanced from the root to the outer edge (normal pressure, T = 100°C); (d) dawsonite preserved well and the mineral surface is relatively regular (P = 4 MPa, T = 80°C); (e) dawsonite with no obvious corrosion (P = 4 MPa, T = 100°C); (f) the surface of dawsonite was dissolved, the edges of the crystal were no longer clear, and the surface was covered by newly precipitated minerals (P = 4 MPa, T = 120°C); (g) the shape of dawsonite aggregate remained intact, but the crystal edges were no longer distinct and the surface was attached by fine new minerals (P = 7.3 MPa, T = 120°C); (h) radial dawsonite aggregate, the edges of individual crystals were more blurred, and the columnar shape was further lost (P = 7.3 MPa, T = 140°C); (i) dawsonite crystals were almost completely turned grayish white, and the aggregates dissolved from the outer edge of the columnar crystal to the root (P = 7.3 MPa, T = 160°C).

weak. At normal pressure, dawsonite began to undergo a large amount of dissolution at 80°C, forming a dissolution hole. At the same time, its energy spectrum composition began to change; C and Na element peak intensity began to weaken; the peak intensity of the Al and O element began to increase (Fig. 7(b)). When the temperature increased to 100°C, dawsonite had a higher degree of dissolution. The peak intensity of the C and O elements on the energy spectrum was further weakened. In contrast, the peak intensity of the Al and Na elements was further enhanced (Fig. 7(c)), which indicated that the composition of the dissolved residue in the photo was changed and no longer had the elemental composition of the mineral of dawsonite. The content of dawsonite was 0 at normal pressure (Fig. 7(d)), indicating that there was no dawsonite in the sandstone sample after the reaction. This demonstrated that the dawsonite in the photograph was completely dissolved, and the crystal structure was completely destroyed.

Under the experimental pressure of 4 MPa, dawsonite was well preserved at 80°C, and the peak characteristics of the C, O, Na, and Al elements in the energy spectrum also indicated that it has typical characteristics of dawsonite composition (Fig. 7(e)). Dawsonite characteristics at 100°C (Fig. 7(f)) were similar to those of dawsonite at 80°C, indicating that it did not undergo dissolution and its composition was not changed. When the temperature increased to 120°C (Fig. 7(g)), dawsonite began to corrode, and new minerals appeared on the mineral surface. However, the peaks of the C and O elements in the energy spectrum were significantly reduced, and only the strong peaks of the Al and Na elements were present. The XRD analysis data also showed that dawsonite content at 4 MPa experimental pressure decreased with increasing temperature compared to that of original sandstone sample (Fig. 7(h)). The content of dawsonite at 100°C and 120°C decreased to 0, which indicated that the structure of dawsonite in the two groups of experiments observed under scanning electron microscopy was severely damaged, the crystal structure of dawsonite was destroyed or altered, resulting in the inability of XRD diffraction to detect the presence of dawsonite.

Under the experimental pressure of 7.3 MPa, when the temperature was 120°C, dawsonite pseudomorph produced radially in Fig. 7(i) had only strong Al and O elemental spectral peak characteristics. Its composition was almost only Al and O elements with small amounts of C, Na, and Si. XRD analysis showed that the amount of dawsonite in the sandstone samples after the experiment was only slightly lower (6%) than that of the starting sandstone samples (7%), indicating that the elemental composition of dawsonite changed almost completely. However, its crystal structure still relatively preserved, allowing XRD analysis to detect its presence in sandstone. The same result was obtained at 140°C. The elemental composition of the dawsonite pseudomorph in Fig. 7(j) consisted almost entirely of Al and O elements with a small amount of C, Na, and Si elements. After the reaction, the amount of dawsonite in the sandstone was further reduced but still contained (1%). When the temperature increased to 160°C, the elemental composition of dawsonite pseudomorph further changed: the Al and O elements still dominated; the Fe element replaced the C and Na elements; and it contained a small amount of Si (Fig. 7(k)). The increased temperature also reduced the amount of dawsonite in the sandstone to zero (Fig. 7(l)), which meant that the mineral seen under scanning electron microscopy not only changed completely in composition but also its crystal structure completely transformed or destroyed.

4 Discussion

4.1 Correction of CO_2 partial pressure

As shown in Fig. 1, the pressure monitored in the experiment is the total pressure of the system. To explore the effect of CO_2 partial pressure on CO_2-water-dawsonite-bearing sandstone interaction, the CO_2 fugacity of the vapor phase in the system was calculated by using the Peng–Robinson equation of state (PR-EoS) (Peng and Robinson, 1976) combined with the van der Waals 1-fluid mixing rule. The PR-EoS is selected because of its simplicity and its widespread use in chemical engineering (Valtz et al., 2004). The functional form of the PR-EoS can be expressed as:

$$P = \frac{RT}{V - b_m} - \frac{a_m}{V^2 + 2Vb_m - b_m^2}, \tag{13}$$

where P, T, and V are pressure, temperature, and molar volume of the system, and R is the ideal gas constant. For mixtures, parameters a_m and b_m are related to the pure component parameters and the mixture composition through a mixing rule. The van der Waals one-fluid mixing rules are applied here, and the parameters a_m and b_m are presented as:

$$a_m = \sum_i \sum_j x_i x_j a_{ij}, \tag{14}$$

$$b_m = \sum_i x_i b_i, \tag{15}$$

where

$$a_{ij} = \sqrt{a_i a_j}(1 - k_{ij}), \tag{16}$$

where x_i and x_j are the mole fractions of component i and j, a_i and a_j is the attraction parameter of pure component i and j, b_i is the repulsion parameter of pure component i, k_{ij} is a binary interaction parameter. For the pure substance, the attraction parameter a_i, and repulsion parameter b_i are determined by the following set of equations:

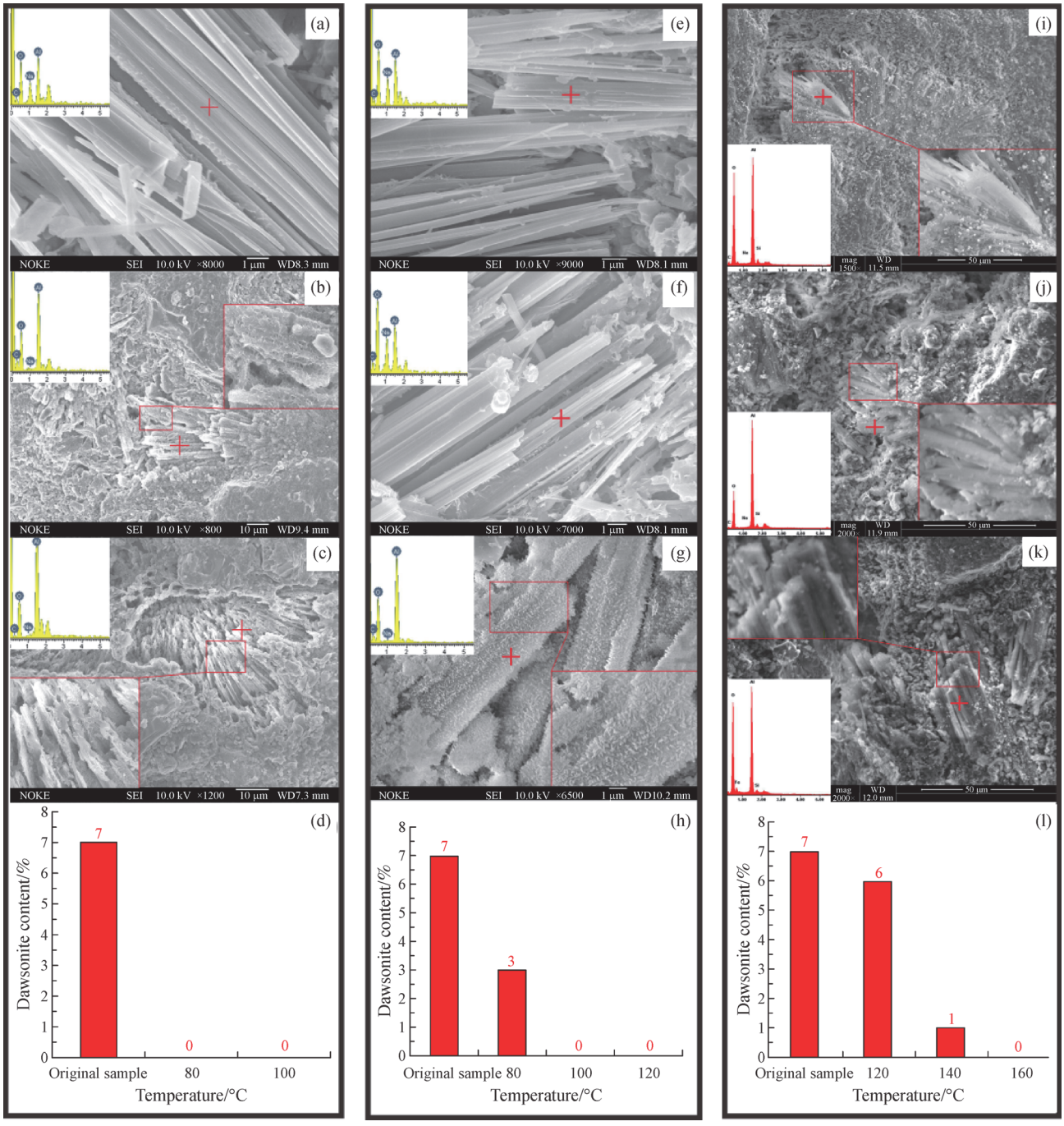

Fig. 7 The composition and content evolution of dawsonite. (a) SEM photo of dawsonite in original sample, and the energy spectrum at the marked point; (b) SEM photo of dawsonite in sandstone at normal pressure 80°C, and the energy spectrum at the marked point; (c) SEM photo of dawsonite in sandstone at normal pressure 100°C, and the energy spectrum at the marked point; (d) the content of dawsonite under the experiment of normal pressure; (e) SEM photo of dawsonite in sandstone at 4 MPa 80°C, and the energy spectrum at the marked point; (f) SEM photo of dawsonite in sandstone at 4 MPa 100°C, and the energy spectrum at the marked point; (g) SEM photo of dawsonite in sandstone at 4 MPa 120°C, and the energy spectrum at the marked point; (h) the content of dawsonite under the experimental pressure of 4 MPa; (i) SEM photo of dawsonite in sandstone at 7.3 MPa 120°C, and the energy spectrum at the marked point; (j) SEM photo of dawsonite in sandstone at 7.3 MPa 140°C, and the energy spectrum at the marked point; (k) SEM photo of dawsonite in sandstone at 7.3 MPa 160°C, and the energy spectrum at the marked point; (h) the content of dawsonite under the experimental pressure of 7.3 MPa.

$$a_i = 0.45724\frac{(RT_{ci})^2}{P_{ci}}\alpha(T), \quad (17)$$

$$b_i = 0.07780\frac{RT_{ci}}{P_{ci}}, \quad (18)$$

where T_{ci} and P_{ci} are the critical temperature and pressure of component i. In this work, the generalized alpha function, $\alpha(T)$, proposed by Coquelet et al. (2004), is selected to accurately represent the vapor pressures of pure compounds:

for $T_{ri} < 1$,

$$\alpha(T) = \exp\left[c_1\left(1-\frac{T_i}{T_{ci}}\right)\right] \times \left[1+c_2\left(1-\sqrt{\frac{T_i}{T_{ci}}}\right)^2 + c_3\left(1-\sqrt{\frac{T_i}{T_{ci}}}\right)^3\right]^2, \quad (19)$$

for $T_{ri} > 1$,

$$\alpha(T) = \exp\left[c_1\left(1-\frac{T_i}{T_{ci}}\right)\right], \quad (20)$$

where T_{ri} is the reduced temperature (T/T_{ci}), c_1, c_2, and c_3 are correlated to the acentric factor ω,

$$c_1 = 1.3569\omega^2 + 0.9957\omega + 0.4077, \quad (21)$$

$$c_2 = -11.2986\omega^2 + 3.5590\omega - 0.1146, \quad (22)$$

$$c_3 = 11.7802\omega^2 - 3.8901\omega + 0.5033. \quad (23)$$

At thermodynamic equilibrium, the fugacity coefficient φ of a component in a mixture can be obtained as:

$$\ln\varphi_i = \frac{b_i}{b_m}\left(\frac{PV}{RT}-1\right) - \ln\frac{P(V-b_m)}{RT} + \frac{a_m}{2\sqrt{2}b_m RT} \times \left[\frac{2}{a_m}\sum_j x_j a_{ij} - \frac{b_i}{b_m}\right]\ln\left[\frac{V+(1-\sqrt{2})b_m}{V+(1+\sqrt{2})b_m}\right]. \quad (24)$$

And the fugacity f_i of component i in a mixture can be calculated by:

$$f_i^V = \varphi_i P x_i = f_i^L, \quad (25)$$

where f_i^V and f_i^L are the fugacity of component i in the vapor and liquid phases. The vapor fugacity of each component calculated by the above equation must be equal in the liquid phase at thermodynamic equilibrium, which will be more representative of the pressure applied to the minerals in the sandstone immersed in the experimental solution. Due to the defects of the experimental apparatus, the vapor phase in the reaction process was not sampled and analyzed. Therefore, the molar fractions of H_2O and CO_2 used for the calculations were taken from Zhao and Lvov (2016), which provided the molar fractions of H_2O and CO_2 of the CO_2–H_2O system at temperatures of 273–623 K and pressures of 0.1–200 MPa. The parameters used for the calculation and the corrected CO_2 fugacity values are listed in Table 3.

4.2 Formation of new minerals and dissolution of dawsonite

During the water-rock interaction process, the dissolution of the initial minerals in the sandstone releases various ions to the solution (Hellevang et al., 2010; Elidemir and Güleç, 2018; Li et al., 2018; Yuan et al., 2019). This behavior provides space for the generation of new minerals and the ions needed for their precipitation (Li et al., 2018; Yuan et al., 2019). At the same time that dawsonite dissolved, the energy spectrum analysis showed that its constituent elements were also constantly changing, and new mineral deposits appeared on the surface of the mineral. Figure 8 was a graph showing the elemental composition evolution of dawsonite after the reaction. At 0 MPa CO_2 partial pressure (Fig. 8(a)), with the increase of temperature, the content of C and Na in dawsonite began to decrease gradually at 80°C, while the content of Al and O increased continuously. The final elemental composition consisted of almost Al and O, containing a small amount of C element, and its average atomic ratio was Al:O:C = 30.35:61.66:8.09. At 4 MPa experimental pressure (Fig. 8(b)), the elemental composition of dawsonite at f_{CO_2} = 3.9 MPa and T = 80°C was similar to that of the

Table 3 The parameters used for the calculation and the corrected CO_2 fugacity values

P/MPa	T/K	x		P_c/MPa		T_c/K		ω		k_{12}	f_{CO_2}/MPa
		CO_2	H_2O	CO_2	H_2O	CO_2	H_2O	CO_2	H_2O		
4	353.15	0.984	0.016	7.383	22.048	304.21	647.30	0.2236	0.3442	0.165	3.9
4	373.15	0.968	0.032	7.383	22.048	304.21	647.30	0.2236	0.3442	0.165	3.8
4	393.15	0.939	0.061	7.383	22.048	304.21	647.30	0.2236	0.3442	0.165	3.7
7.3	393.15	0.959	0.041	7.383	22.048	304.21	647.30	0.2236	0.3442	0.165	6.9
7.3	413.15	0.931	0.069	7.383	22.048	304.21	647.30	0.2236	0.3442	0.165	6.7
7.3	433.15	0.887	0.113	7.383	22.048	304.21	647.30	0.2236	0.3442	0.165	6.4

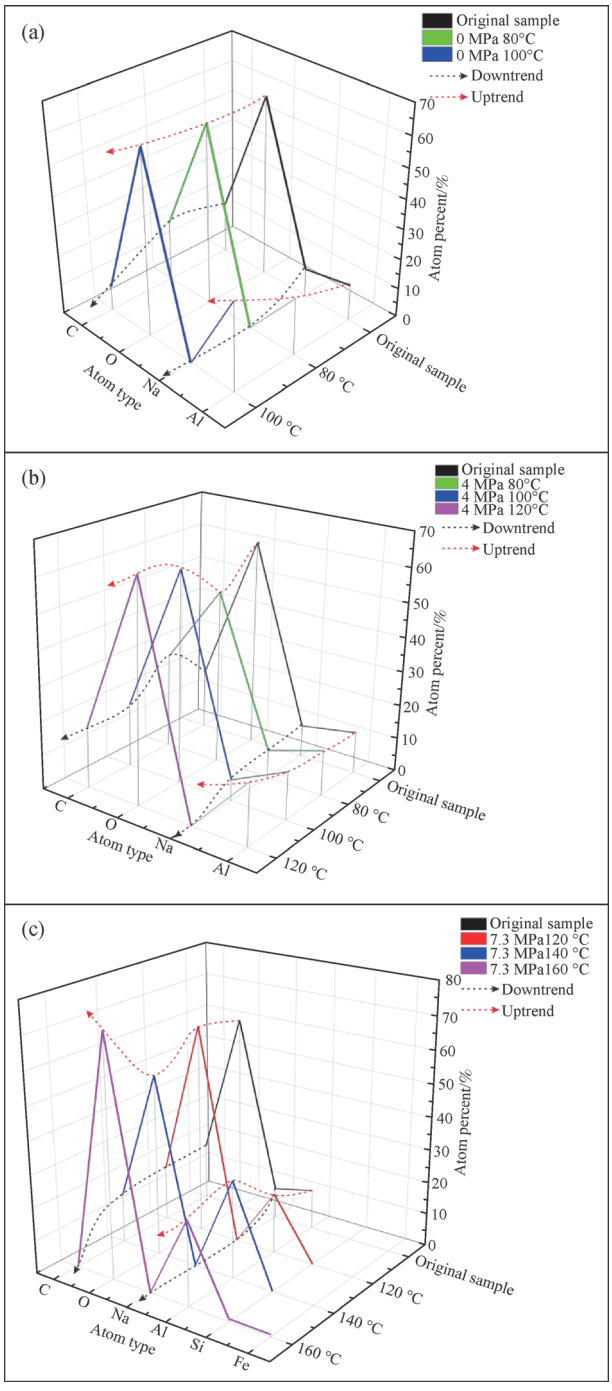

Fig. 8 Elemental composition evolution of dawsonite after the reaction.

original dawsonite. The C and O elements in dawsonite at f_{CO_2} = 3.8 MPa and T = 100°C began to decrease, and Al:O:C:Na = 13.95:61.25:18.61:6.18. At 120°C and the CO_2 fugacity of 3.7 MPa, the content of Na element in dawsonite was reduced to 0; the content of C element further decreased; the content of Al and O elements further increased; Al:O:C = 18.12:64.02:17.94. At 7.3 MPa experimental pressure (Fig. 8(c)), the Na element in dawsonite was sharply reduced to 0 at f_{CO_2} = 6.9 MPa and T = 120°C, and the C element also continuously decreased. The Si element began to appear in the energy spectrum. As the temperature increased to 160°C and the CO_2 fugacity of 6.4 MPa, Si element further increased; C and Na elements were replaced by Fe element; and Al:O:Si:Fe = 25.74:72.7:0.83:0.73.

The crystal structure of dawsonite is a distorted octahedron composed of carbon-aluminate chains with $[Al_2(OH)_4(CO_3)_2]^{2-}$ as the basic unit (Frost et al., 2015; Li et al., 2018). CO_3^{2-} is located at the two ends of the carbon-aluminum chain. Na^+ is located outside the carbon-aluminum chain and connected to multiple carbon-aluminum chains (Fernández-Carrasco et al., 2005; Frost et al., 2015; Li et al., 2018). With the increase of temperature, dawsonite continues to be corroded under different CO_2 pressure conditions. As a consequence, its elemental composition changed continuously, the content of C and Na elements decreased continuously, and the content of Al and O elements increased continuously, too. This also explained that in the aqueous solution of each group of experiments, the ionic dissolution rate of K^+ and Na^+ released from the continuously dissolving feldspar was increased, and the Al^{3+} in solution was precipitated continuously, resulting in the increasing strength of the peak of Al element in the energy spectrum composition of dawsonite. Furthermore, the ion dissolution rate of Al^{3+}, which should be more significantly increased, was reduced or almost zero. Previous experiments showed that dawsonite gradually hydrolyzed to produce aluminum hydroxides, boehmite, as the environmental conditions change (Stoica and Pérez-Ramírez, 2010; Li et al., 2018). Boehmite, AlO(OH), with Al:O = 1:2, while according to the atomic ratio of dawsonite in each group of experiments, the atomic ratio is close to Al:O = 1:3, which is the same as another Al hydroxide: gibbsite, $Al(OH)_3$, with Al:O = 1:3 (Raybaud et al., 2001; Yang et al., 2018b). Therefore, we concluded that the mineral formed after the dissolution of dawsonite in those experiments was gibbsite. Dawsonite began to transform to gibbsite at a temperature of 80°C under the CO_2 partial pressure of 0 MPa and began to transform to gibbsite at 120°C and the CO_2 fugacity of 3.7 MPa. While at the CO_2 fugacity of 6.9 MPa, dawsonite was almost completely converted to gibbsite at a temperature of 120°C.

4.3 Comprehensive analysis of the dissolution mechanism of dawsonite

The minerals in sandstone reservoirs were not only affected by temperature but also by pressure, fluid type, fluid salinity, and other factors (Bakhshi et al., 2018; Ajayi et al., 2019; Yu et al., 2019; Yuan et al., 2019). According to the experimental results, dawsonite gradually dissolved with the increase of the reaction temperature, but the dissolution gradually occurred instead of being completed

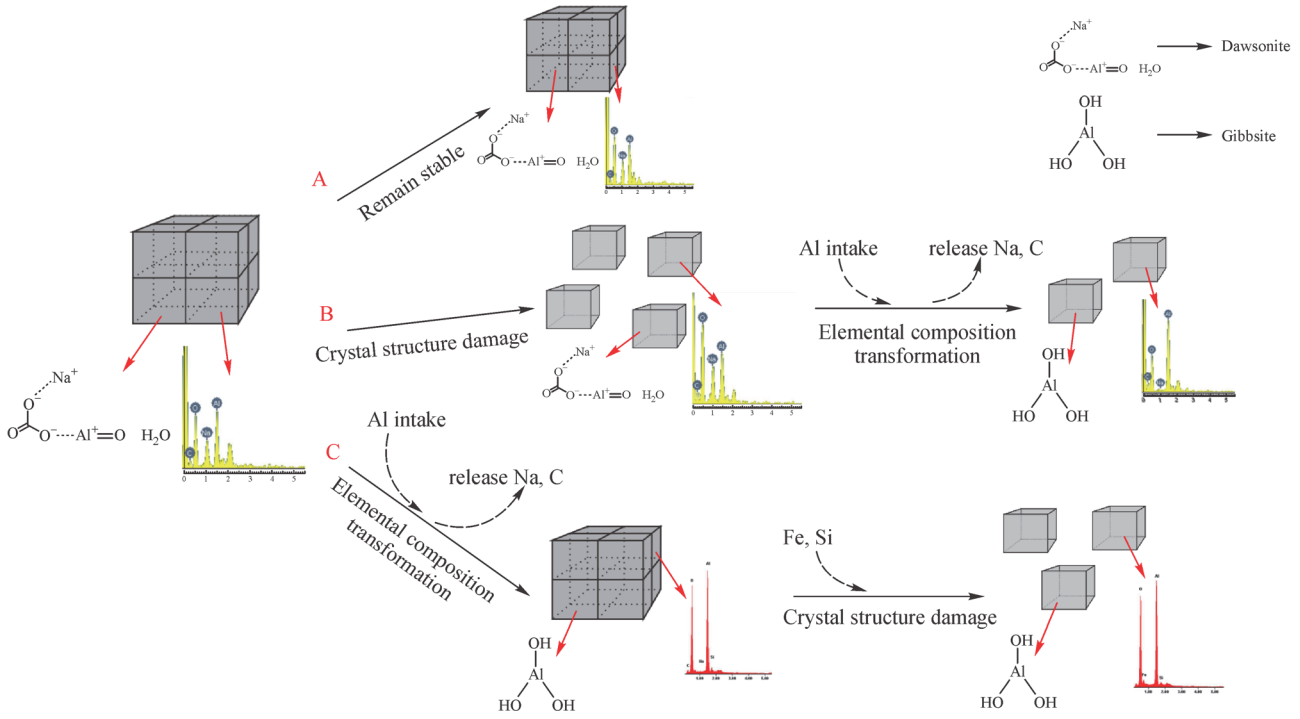

Fig. 9 Dissolution patterns of dawsonite under different CO_2 partial pressures and temperature conditions.

at once (Huggins and Green, 1973). The experimental results suggested that the dissolution extent and mechanism of dawsonite under different CO_2 partial pressure conditions were different. Under the CO_2 partial pressure of 0 MPa, dawsonite was almost completely corroded at 80°C, and its content was 0 indicated by XRD analysis data, and its elemental composition detected the only slight change. This indicated that the crystal structure of dawsonite at 80°C was completely damaged by the dissolution, which showed that dawsonite observed under the scanning electron microscope was corroded to produce a large number of dissolution pits, and the composition of dawsonite dissolution residue began to change. At 100°C, according to XRD data, the content of dawsonite in the sandstone was also 0, and the composition of the element was further changed by energy spectrum analysis. The dawsonite observed by scanning electron microscopy was corroded more intense, and the mineral morphology was severely damaged, crystal structure characteristics were completely lost, and the composition of the dawsonite element was further changed.

Under the experimental pressure of 4 MPa, the content of 3% was still detected in the sandstone after the reaction at f_{CO_2} = 3.9 MPa and T = 80°C, while dawsonite was still well preserved under the scanning electron microscope, the surface was flat and regular, and dawsonite spectrum was of well feature. At f_{CO_2} = 3.8 MPa and T = 100°C, the content of dawsonite was reduced to 0. The corrosion of dawsonite observed under scanning electron microscopy was still not obvious, and its spectral characteristics were only slightly changed. When the temperature continued to increase to 120°C, and the f_{CO_2} is 3.7 MPa, the content of dawsonite was 0, its spectral characteristics had undergone a significant change, and dawsonite under the scanning electron microscope had been largely corroded, accompanied by a large amount of new minerals attached to its surface. This indicated that the damage of the crystal structure of dawsonite at 4 MPa experimental pressure was still earlier than the transformation of its elemental composition. The crystal structure was damaged at f_{CO_2} = 3.8 MPa and T = 100°C, and its elemental composition changed at f_{CO_2} = 3.7 MPa and T = 120°C.

Under the 7.3 MPa experimental pressure, the content of dawsonite was 6% at f_{CO_2} = 6.9 MPa and T = 120°C, and there was almost no decrease. The energy spectrum characteristics indicated that the elemental composition was completely changed, and the appearance of Si was found. The shape integrity of dawsonite under SEM was well preserved, but the edges between the mineral monomers were no longer clear and became blurred. The content of dawsonite was 1% at f_{CO_2} = 6.7 MPa and T = 140°C, and its elemental composition was further changed, while the mineral edge was observed to be more blurred under scanning electron microscopy. When the temperature was increased to f_{CO_2} = 6.4 MPa and T = 160°C, dawsonite content was reduced to 0, the energy spectrum composition changed more completely, no longer contained C and Na elements, although the mineral shape remained well under scanning electron microscopy, the edges between the single crystal were quite blurry. This

indicated that the compositional transformation of the dawsonite element occurred at f_{CO_2} = 6.9 MPa and T = 120°C, and the damage of its crystal structure occurs at f_{CO_2} = 6.4 MPa and T = 160°C. Therefore, the compositional transformation of dawsonite at 7.3 MPa experimental pressure occurred before the destruction of its crystal structure.

High CO_2 pressures inevitably lead to higher H^+ concentrations, according to Eq. (1) to Eq. (4). Previous studies demonstrated that high H^+ concentrations contributed to the dissolution of dawsonite and other minerals in sandstone (Zerai et al., 2006; Hellevang et al., 2010; Yu et al., 2019; Yuan et al., 2019). Under high CO_2 pressure conditions, while producing more H^+, it also corresponds to a higher CO_2 concentration in the liquid phase, which will induce an inhibitory effect on the dissolution of dawsonite, according to Eq. (11) (Hellevang et al., 2010). Previous studies also indicated that dawsonite under high pCO_2 conditions could remain high thermodynamic stability (Chesworth, 1971; Zhang et al., 2004). And the increase of reaction temperature will reduce the stability of dawsonite, resulting in its crystal structure becomes unstable (Li et al., 2018), and the C and Na elements in the crystal lattice will continuously detach at high temperature (Li et al., 2018). The experimental results showed that under the high CO_2 fugacity (at the experimental pressure of 7.3 MPa), the inhibition effect was remarkable, and the dissolution was mainly the continuous depletion of Na and C in the crystal structure at high temperatures. This residual crystal structure was extremely unstable and will be destroyed with the increased degree of depletion, thereby completely losing the crystal structure characteristics of dawsonite. H^+ is continuously consumed in the solution by the preferential dissolution of readily soluble carbonate minerals such as calcite and ankerite (Arvidson et al., 2003; Gaus et al., 2008; Kampman et al., 2009; Yu et al., 2017; Yuan et al., 2019), resulting in a continuous decrease in its concentration. The inhibition effect was relatively low, at 4 MPa experimental pressure. And the H^+ ions in the solution continuously destroyed the crystal structure so that the original crystal structure was lost, as shown by the reduction of the content of dawsonite minerals on XRD data. At f_{CO_2} = 3.8 MPa, T = 100°C and f_{CO_2} = 3.7 MPa, T = 120°C, due to the increase of temperature and the decrease of CO_2 fugacity, the H^+ concentration was relatively low, and the mineral corrosion continuously consumed H^+, which caused the damage of H^+ to the crystal structure of dawsonite to decrease after a period of reaction. Under the influence of CO_2 pressure and temperature, dawsonite began to suffer chemical depletion of Na and C. On the other hand, the distilled water used in our experiments will form an unsaturated solution environment for the minerals in the sandstone after the start of the reaction. This unsaturated solution environment will promote the dissolution of the minerals to achieve an equilibrium between solution and minerals. At 0 MPa CO_2 pressure, the dawsonite immersed in unsaturated distilled water will dissolve continuously due to the unsaturated state between the solution and the mineral.

In summary, there are two ways to reduce the stability of dawsonite, one is the transformation of its constituent elements, and the other is the damage of its crystal structure. Studies by Burnham et al. (2015) showed that the degree of decomposition of dawsonite at high CO_2 partial pressure was lower than that at low CO_2 partial pressure. Under different CO_2 partial pressures and temperature conditions, the occurrence order of elemental composition transformation and crystal structure damage was different. And under high CO_2 partial pressure conditions, the temperature was higher at which elemental composition transformation and crystal structure damage occurred. Based on the experimental results, three types of the dissolution patterns of dawsonite under different CO_2 fugacity and temperature conditions were summarized (Fig. 9). Among them, mode A represents the development mode of dawsonite under low CO_2 pressure and temperature. The temperature and pressure of the environment of dawsonite are not high enough to cause elemental composition transformation and crystal structure damage, which corresponds to f_{CO_2} = 0 MPa, $T < 80$°C; f_{CO_2} = 3.8 MPa, $T < 100$°C; f_{CO_2} = 6.9 MPa, $T < 120$°C in this paper. Mode B represents the evolution of dawsonite at moderate CO_2 pressure and temperature, indicating that dawsonite under this condition preferentially corrodes the crystal structure, and its elemental composition gradually dissolves when the crystal structure is severely damaged. This corresponds to f_{CO_2} = 0 MPa, $T > 80$°C; f_{CO_2} = 3.8 MPa, $T > 100$°C. Mode C represents the evolution of dawsonite at high CO_2 pressure and temperature, indicating that dawsonite under this condition will first dissolve the constituent elements, and then the crystal structure will be corroded. This corresponds to f_{CO_2} = 6.9 MPa, $T > 120$°C.

4.4 Implications

For CCS projects, the CO_2 injected into the reservoir will eventually be stored in the form of dawsonite-based minerals (Zerai et al., 2006; Li et al., 2018; Ajayi et al., 2019). The stability of dawsonite in the reservoir will become an important factor affecting the long-term safety of CCS projects (DePaolo and Cole, 2013; IPCC, 2014; Li et al., 2017). This study shows that high CO_2 pressure is favorable for maintaining the stability of dawsonite, while high formation temperature is unfavorable for maintaining the stability of dawsonite. The formation temperature and pressure of the underground reservoir both increase with the increase of depth. The depths of CO_2 reservoirs selected in ongoing CCS projects (such as Sleipner) are mostly in the range of 1000–2000 m, and a few reach 2500 m (Bachu, 2002; Benson and Cole, 2008; Oelkers and Cole, 2008; IPCC, 2014; Aminu et al., 2017). Although the

geothermal gradient of each basin is different, the temperature of the formation does not exceed 100°C in this depth range. The formation pressure can reach more than 10 MPa, and even over 30 MPa. By injecting a large amount of CO_2 gas, such a reservoir can reach a higher CO_2 partial pressure and maintain a lower temperature, which can promote the formation of dawsonite and maintain a stable state. It indicates that CO_2 trapping and storage within this depth range can ensure that dawsonite is stable. Therefore, CO_2 can be effectively stored, and the long-term safety of CO_2 geological storage is guaranteed.

5 Conclusions

The CO_2-water-dawsonite-bearing sandstone interaction experiments were performed under different temperature and CO_2 pressures revealing a new understanding of the preservation conditions of dawsonite. The stability of dawsonite showed a tendency to increase with the increasing partial pressure of CO_2, and there are two ways to reduce the stability of dawsonite: the transformation of elemental composition and the damage of crystal structure.

Dawsonite under high CO_2 partial pressure shows relatively high thermodynamic stability. It is supported by the experiments performed under high CO_2 partial pressure. The temperature is also higher required for the dissolution of dawsonite (including the transformation of elemental composition and the dissolution of crystal structure). Under the condition of 0 MPa CO_2 partial pressure, dawsonite begins to completely corrode the crystal structure at 80°C, and its composition dissolves at 100°C. Under the experimental pressure of 4 MPa, the crystal structure of dawsonite completely corroded at f_{CO_2} = 3.8 MPa and T = 100°C, and its composition begins to dissolve at f_{CO_2} = 3.7 MPa and T = 120°C and to form gibbsite. Under the experimental pressure of 7.3 MPa, the crystallite structure of dawsonite completely corrodes at a higher temperature (f_{CO_2} = 6.4 MPa, T = 160°C), and the dissolution of its constituents occurs at f_{CO_2} = 6.9 MPa and T = 120°C, and it transforms into gibbsite.

The experiments indicated there exists three dissolution evolution patterns of dawsonite. Under different CO_2 partial pressures, the dissolution evolution pattern of dawsonite is different. Under medium and low-pressure conditions, if the ambient temperature is higher than the crystal structure corrosion temperature of dawsonite, dawsonite will first undergo the corrosion of the crystal structure. When the temperature continues to increase beyond the dissolution temperature of the component of dawsonite, its component will dissolve and begin to transform to gibbsite. Under high-pressure conditions, dawsonite will first dissolve the constituents, forming gibbsite, followed by the corrosion of the crystal structure.

Acknowledgements The authors thank the editors and two anonymous reviewers for their careful check and helpful comments and modification of the manuscript. This study is financially supported by the National Natural Science Foundation of China (Grants Nos. 42072130 and 41872152).

References

Ajayi T, Gomes J S, Bera A (2019). A review of CO_2 storage in geological formations emphasizing modeling, monitoring and capacity estimation approaches. Petrol Sci, 16(5): 1028–1063

Álvarez-Ayuso E, Nugteren H W (2005). Synthesis of dawsonite: a method to treat the etching waste streams of the aluminium anodising industry. Water Res, 39(10): 2096–2104

Aminu M D, Nabavi S A, Rochelle C A, Manovic V (2017). A review of developments in carbon dioxide storage. Appl Energy, 208: 1389–1419

Arvidson R S, Ertan I E, Amonette J E, Luttge A (2003). Variation in calcite dissolution rates: a fundamental problem? Geochim Cosmochim Acta, 67(9): 1623–1634

Bachu S (2002). Sequestration of CO_2 in geological media in response to climate change: road map for site selection using the transform of the geological space into the CO_2 phase space. Energy Convers Manage, 43(1): 87–102

Bakhshi P, Kharrat R, Hashemi A, Zallaghi M (2018). Experimental evaluation of carbonated waterflooding: a practical process for enhanced oil recovery and geological CO_2 storage. Greenh Gases Sci Techn, 8(2): 238–256

Baker J C, Bai G P, Hamilton P J, Golding S D, Keene J B (1995). Continental-scale magmatic carbon dioxide seepage recorded by dawsonite in the Bowen-Gunnedah-Sydney Basin system, eastern Australia. J Sediment Res, 65A: 522–530

Benson S M, Cole D R (2008). CO_2 sequestration in deep sedimentary formations. Elements, 4(5): 325–331

Burnham A K, Levchenko A, Herron M M (2015). Analysis, occurrence, and reactions of dawsonite in AMSO well CH-1. Fuel, 144: 259–263

Chesworth W (1971). Laboratory synthesis of dawsonite and its natural occurrences. Nat Phys Sci (Lond), 231(19): 40–41

Coquelet C, Chapoy A, Richon D (2004). Development of a new alpha function for the Peng–Robinson Equation of state: comparative study of alpha function models for pure gases (natural gas components) and water-gas systems. Int J Thermophys, 25(1): 133–158

Dejean A, Céréghino R, Carpenter J M, Corbara B, Hérault B, Rossi V, Leponce M, Orivel J, Bonal D (2011). Climate change impact on neotropical social wasps. PLoS One, 6(11): e27004

DePaolo D J, Cole D R (2013). Geochemistry of geologic carbon sequestration: an overview. Rev Mineral Geochem, 77(1): 1–14

Dickinson W R (1970). Interpreting detrital modes of graywacke and arkose. J Sediment Res, 40: 695–707

Dong L, Liu L, Qu X, Yang H, Li F, Liu N, Guo X (2009). Crystal characteristics and genesis of dawsonite of the Qingshankou formation in the Honggang Oilfield in the Honggang Terrace of Songliao Basin. J Jilin U, 39: 1031–1104 (in Chinese)

Elidemir S, Güleç N (2018). Geochemical characterization of geothermal systems in western Anatolia (Turkey): implications for CO_2 trapping

mechanisms in prospective CO_2-EGS sites. Greenh Gases Sci Techn, 8(1): 63–76

Fernández-Carrasco L, Puertas F, Blanco-Varela M, Vázquez T, Rius J (2005). Synthesis and crystal structure solution of potassium dawsonite: an intermediate compound in the alkaline hydrolysis of calcium aluminate cements. Cement Concrete Res, 35(4): 641–646 .

Frost R L, López A, Scholz R, Sampaio N P, de Oliveira F A (2015). SEM, EDS and vibrational spectroscopic study of dawsonite NaAl $(CO_3)(OH)_2$. Spectrochim Acta A Mol Biomol Spectrosc, 136(Pt B): 918–923

Gao Y,Liu L (2006). Carbon-oxygen isotopic characteristics of authigenic dawsonite and its genetic significance. Geol J China U, 12(4): 522–529 (in Chinese)

Gao Y, Liu L, Hu W (2009). Petrology and isotopic geochemistry of dawsonite-bearing sandstones in Hailar Basin, Northeastern China. Appl Geochem, 24(9): 1724–1738

Gao Y, Liu L, Qu X, Liu N (2008). Petrologic characteristics of dawsonite—bearing sandstones in Wuerxun Sag of Hailar Basin and Gudian CO_2 gasfield in Songliao Basin. J Palaeogeograph, 10: 111–123 (in Chinese)

Gaus I (2010). Role and impact of CO_2–rock interactions during CO_2 storage in sedimentary rocks. Int J Greenh Gas Control, 4(1): 73–89

Gaus I, Audigane P, André L, Lions J, Jacquemet N, Durst P, Czernichowski-Lauriol I, Azaroual M (2008). Geochemical and solute transport modelling for CO_2 storage, what to expect from it? Int J Greenh Gas Control, 2(4): 605–625

Gunnemyr M (2019). Causing global warming. Ethical Theory Moral Pract, 22(2): 399–424

Gysi A P, Stefánsson A (2008). Numerical modelling of CO_2-water-basalt interaction. Mineral Mag, 72(1): 55–59

Hellevang H, Declercq J, Kvamme B, Aagaard P (2010). The dissolution rates of dawsonite at pH 0.9 to 5 and temperatures of 22, 60 and 77 °C. Appl Geochem, 25(10): 1575–1586

Holloway S (2005). Underground sequestration of carbon dioxide—a viable greenhouse gas mitigation option. Energy, 30(11–12): 2318–2333

Holloway S, Savage D (1993). The potential for aquifer disposal of carbon dioxide in the UK. Energy Convers Manage, 34(9–11): 925–932

Huggins C W, Green T E (1973). Thermal decomposition of dawsonite. Am Mineral, 58: 548–550

IPCC (2014).Climate Change 2013—The Physical Science Basis: Working Group I Contribution to the Fifth Assessment Report of the Intergovernmental Panel on Climate Change. Cambridge: Cambridge University Press

Jiang H, Shen P, Li X, Huang W, Cai J, Ju B,Guo J (2008). Study into technologies for estimating theoretical volume of CO_2 stored underground worldwide. Sino-Global Energ, 13(2): 93–99 (in Chinese)

Johnson J W (2009). Integrated modeling, monitoring, and site characterization to assess the isolation performance of geologic CO_2 storage: Requirements, challenges, and methodology. Energ Procedia, 1(1): 1855–1861

Johnson J W, Nitao J J, Knauss K G (2004). Reactive transport modelling of CO_2 storage in saline aquifers to elucidate fundamental processes, trapping mechanisms and sequestration partitioning. Geol Soc Lond Spec Publ, 233(1): 107–128

Kampman N, Bickle M, Becker J, Assayag N, Chapman H (2009). Feldspar dissolution kinetics and Gibbs free energy dependence in a CO_2-enriched groundwater system, Green River, Utah. Earth Planet Sci Lett, 284(3-4): 473–488

Karl T R, Melillo J M, Peterson T C, Hassol S J (2009). Global Climate Change Impacts in the United States. Cambridge: Cambridge University Press

Karl T R, Trenberth K E (2003). Modern global climate change. Science, 302(5651): 1719–1723

Kharaka Y K, Cole D R, Thordsen J J, Kakouros E, Nance H S (2006). Gas–water–rock interactions in sedimentary basins: CO_2 sequestration in the Frio Formation, Texas, USA. J Geochem Explor, 89(1–3): 183–186

Korbøl R, Kaddour A (1995). Sleipner vest CO_2 disposal-injection of removed CO_2 into the utsira formation. Energy Convers Manage, 36(6-9): 509–512

Lechat K, Lemieux J M, Molson J, Beaudoin G, Hébert R (2016). Field evidence of CO_2 sequestration by mineral carbonation in ultramafic milling wastes, Thetford Mines, Canada. Int J Greenh Gas Control, 47: 110–121

Li F, Cao Y, Li W, Zhang L (2018). CO_2 mineral trapping: Hydrothermal experimental assessments on the thermodynamic stability of dawsonite at 4.3 MPa pCO_2 and elevated temperatures. Greenh Gases Sci Techn, 8(1): 77–92

Li F, Li W (2017). Petrological record of CO_2 influx in the Dongying Sag, Bohai Bay Basin, NE China. Appl Geochem, 84: 373–386

Li F, Li W, Yu Z, Liu N, Yang H, Liu L (2017). Dawsonite occurrences related to the age and origin of CO_2 influx in sandstone reservoirs: a case study in the Songliao Basin, NE China. Geochem Geophys Geosyst, 18(1): 346–368

Liu L, Hong Y, Hocker J E, Shafer M A, Carter L M, Gourley J J, Bednarczyk C N, Yong B, Adhikari P (2012). Analyzing projected changes and trends of temperature and precipitation in the southern USA from 16 downscaled global climate models. Theor Appl Climatol, 109(3–4): 345–360

Melillo J M (2014).Climate change impacts in the United States, highlights: US national climate assessment. Washington D.C.: Government Printing Office

Moore J, Adams M, Allis R, Lutz S, Rauzi S (2005). Mineralogical and geochemical consequences of the long-term presence of CO_2 in natural reservoirs: an example from the Springerville–St. Johns Field, Arizona, and New Mexico, U.S.A. Chem Geol, 217(3–4): 365–385

Oelkers E H, Cole D R (2008). Carbon dioxide sequestration a solution to a global problem. Elements, 4(5): 305–310

Okuyama Y (2014). Dawsonite-bearing carbonate veins in the Cretaceous Izumi Group, SW Japan: a possible natural analogue of fracture formation and self-sealing in CO_2 geological storage. Energ Procedia, 63: 5530–5537

Okuyama Y, Nakashima Y, Sasaki M, Ueda A (2011). Do the sedimentary strata have power to neutralize leaking CO_2? A natural analogue study on past CO_2 invasion and carbonate precipitation in the Cretaceous Izumi Group, SW Japan. Energ Procedia, 4: 4953–4960

Peng D Y, Robinson D B (1976). A new two-constant equation of state.

Ind Eng Chem Fundam, 15(1): 59–64

Raza A, Gholami R, Rezaee R, Rasouli V, Bhatti A A, Bing C H (2018). Suitability of depleted gas reservoirs for geological CO_2 storage: a simulation study. Greenh Gases Sci Techn, 8(5): 876–897

Raybaud P, Digne M, Iftimie R, Wellens W, Euzen P, Toulhoat H (2001). Morphology and surface properties of boehmite (γ-AlOOH): a density functional theory study. J Catal, 201(2): 236–246

Shevalier M, Nightingale M, Johnson G, Mayer B, Perkins E, Hutcheon I (2009). Monitoring the reservoir geochemistry of the Pembina Cardium CO_2 monitoring project, Drayton Valley, Alberta. Energ Procedia, 1(1): 2095–2102

Stoica G, Pérez-Ramírez J (2010). Stability and inter-conversion of synthetic dawsonites in aqueous media. Geochim Cosmochim Acta, 74(24): 7048–7058

Valtz A, Chapoy A, Coquelet C, Paricaud P, Richon D (2004). Vapour–liquid equilibria in the carbon dioxide–water system, measurement and modelling from 278.2 to 318.2 K. Fluid Phase Equilib, 226: 333–344

Wang K, Xu T, Tian H, Wang F (2016). Impacts of mineralogical compositions on different trapping mechanisms during long-term CO_2 storage in deep saline aquifers. Acta Geotech, 11(5): 1167–1188

Worden R H (2006). Dawsonite cement in the Triassic Lam Formation, Shabwa Basin, Yemen: a natural analogue for a potential mineral product of subsurface CO_2 storage for greenhouse gas reduction. Mar Pet Geol, 23(1): 61–77

Xu T, Apps J A,Pruess K, (2003). Reactive geochemical transport simulation to study mineral trapping for CO_2 disposal in deep arenaceous formations. J Geophys Res Sol Ea, 108

Xu T, Apps J A, Pruess K (2004). Numerical simulation of CO_2 disposal by mineral trapping in deep aquifers. Appl Geochem, 19(6): 917–936

Yang Z, Xu T, Wang F, Yang Y, Li X, Zhao N (2018a). Impact of inner reservoir faults on migration and storage of injected CO_2. Int J Greenh Gas Control, 72: 14–25

Yang H, Liu F, Zhao H, Wu R (2018b). Hydrothermal process of synthetic gibbsite and the characteristics of Na in gibbsite crystal. Chem Pap, 72(12): 3169–3178

Yu Z, Liu K, Liu L, Yang S, Yang Y (2017). An experimental study of CO_2 - oil - brine - rock interaction under *in situ* reservoir conditions. Geochem Geophys Geosyst, 18(7): 2526–2542

Yu Z, Yang S, Liu K, Zhou Q, Yang L (2019). An experimental and numerical study of CO_2–brine-synthetic sandstone interactions under high-pressure (P)–temperature (T) reservoir conditions. App Sci, 9: 3354

Yuan G, Cao Y, Zan N, Schulz H M, Gluyas J, Hao F, Jin Q, Liu K, Wang Y, Chen Z, Jia Z (2019). Coupled mineral alteration and oil degradation in thermal oil-water-feldspar systems and implications for organic-inorganic interactions in hydrocarbon reservoirs. Geochim Cosmochim Acta, 248: 61–87

Zerai B, Saylor B Z, Matisoff G (2006). Computer simulation of CO_2 trapped through mineral precipitation in the Rose Run Sandstone, Ohio. Appl Geochem, 21(2): 223–240

Zhang X, Wen Z, Gu Z, Xu X, Lin Z (2004). Hydrothermal synthesis and thermodynamic analysis of dawsonite-type compounds. J Solid State Chem, 177(3): 849–855

Zhao H, Lvov S N (2016). Phase behavior of the CO_2–H_2O system at temperatures of 273–623 K and pressures of 0.1–200 MPa using Peng-Robinson-Stryjek-Vera equation of state with a modified Wong-Sandler mixing rule: an extension to the CO_2–CH_4–H_2O system. Fluid Phase Equilib, 417: 96–108

Zhou B, Liu L, Zhao S, Ming X, Oelkers E H, Yu Z, Zhu D (2014). Dawsonite formation in the Beier Sag, Hailar Basin, NE China tuff: a natural analog for mineral carbon storage. Appl Geochem, 48: 155–167